Stress evolution during and after sputter deposition of thin Cu–Al alloy films

2008 J. Phys.: Condens. Matter 20 255215

(http://iopscience.iop.org/0953-8984/20/25/255215)

IOP PUBLISHING JOURNAL OF PHYSICS: CONDENSED MATTER

J. Phys.: Condens. Matter **20** (2008) 255215 (6pp) doi:10.1088/0953-8984/20/25/255215

Stress evolution during and after sputter deposition of thin Cu–Al alloy films

M Pletea[1,3], H Wendrock[1], R Kaltofen[1], O G Schmidt[1] and R Koch[2]

[1] Leibniz-Institut für Festkörper- und Werkstoffforschung, Helmholtzstraße 20, D-01069 Dresden, Germany

[2] Institut für Halbleiter- und Festkörperphysik, Johannes Kepler Universität, Altenbergerstrasse 69, A-4040 Linz, Austria

E-mail: T.M.Pletea@ifw-dresden.de

Received 14 January 2008, in final form 28 April 2008
Published 21 May 2008
Online at stacks.iop.org/JPhysCM/20/255215

Abstract

The stress evolution during and after sputter deposition of thin Cu–Al alloy films containing 1 and 2 at.% Al onto oxidized Si(100) substrates has been studied up to thicknesses of 300 nm by means of *in situ* substrate curvature measurements. In order to correlate stress and morphology, the microstructure was investigated by focused ion beam microscopy, scanning electron microscopy, and atomic force microscopy. The evolution of the stress and microstructure of the Cu–Al alloy films is similar to that for sputtered pure Cu films. Film growth proceeds in the Volmer–Weber mode, typical for high mobility metals. It is characterized by nucleation, island, percolation, and channel stages before the films become continuous, as well as lateral grain growth in the compact films. With increasing Al content the overall atom mobility and, thus, the average grain size of the alloy films are reduced. Increase of the sputter pressure from 0.5 to 2 Pa leads to films with larger grain size, rougher surface morphology and higher electrical resistivity.

1. Introduction

Copper is employed as an interconnect material for deep submicron ultralarge scale integration (ULSI) applications, where—due to its lower resistivity, higher stability against failure by electromigration, and improved mechanical properties—it continues to replace aluminum [1, 2]. The use of Cu instead of Al in ULSI manufacturing, however, raises some problems. For instance, unlike upon Al metalization, Cu does not form a self-passivating oxide on its surface. Therefore volatile compounds adhering poorly on dielectrics adsorb on Cu and diffuse into Si to act as recombination centers. Moreover, in the Cu films, considerable grain growth (compared to the case for Al films) occurs even at temperatures as low as room temperature [3]. In order to overcome these technological obstacles, new or modified interconnect materials have to be found which still maintain the most desired properties of Cu—low resistivity and high stability against electromigration [4]. A promising approach for improving the reliability of interconnect materials is the addition of small amounts of other elements (i.e., Al, Au, Ag, Nb, Zn, Mg) to the pure metal films [5]. In recent years, the investigations have focused on thin films of dilute Cu-based alloys as potential materials for replacing the Cu interconnects. Our interest in Cu–Al alloys is motivated by the fact that Al is in the higher priority group of potential alloying elements for Cu interconnect films [5].

Stress migration is another dominant failure mechanism determining reliability and lifetime of interconnects. Therefore, knowledge and control of the stress level developing during and after deposition of Cu-based alloys films is essential for improving their performance. In the literature great attention is paid to the effect of Al addition on corrosion, resistivity, adhesion, and microstructural features (grain size, grain size distribution, texture, etc) of the Cu films [6–9]. However, no systematic studies on the stress evolution during and after deposition of films based on dilute Cu–Al alloys have been performed until now.

In this paper, we report on our study of the stress evolving during and after sputter deposition of thin Cu–Al alloy films on thermally oxidized Si(100) substrates (denoted by SiO_x) for different compositions and thicknesses. In order to identify possible sources of the stress, microstructural investigations by scanning electron microscopy (SEM) and atomic force

[3] Author to whom any correspondence should be addressed.

Table 1. Deposition parameters for Cu and Al to obtain Cu–(1 at.%)Al and Cu–(2 at.%)Al films (for each sputter pressure, the lower and higher Al deposition rates correspond to Cu–(1 at.%)Al and Cu–(2 at.%)Al, respectively).

Material	Sputter pressure (Pa)	Deposition rate (nm min^{-1})	Discharge power (W)
Cu	0.5	27	200
	2.0	8.4	150
Al	0.5	0.39	130
		0.78	300
	2.0	0.12	115
		0.24	240

microscopy (AFM) were additionally performed. The relation between stress, microstructure, and resistivity of Cu–Al thin films will be discussed.

2. Experimental procedure

Thin Cu–Al alloy films of different thicknesses ranging from 3 to 300 nm and two different Al contents (1 and 2 at.%) have been prepared by DC magnetron sputtering onto SiO_x substrates. The base pressure of the sputter system was 10^{-6} Pa. Argon of 99.998% purity was introduced as working gas into the deposition chamber with a mass flow rate of 10 SCCM (cubic centimeter per minute at standard temperature and pressure). The samples were prepared from Cu and Al targets (purity 99.99%) with a diameter of 75 mm and a mean substrate–target distance of 175 mm. The two targets were exposed simultaneously to the Ar plasma cloud. For the present investigation we used sputter pressures of 0.5 and 2.0 Pa and two different deposition rates of Cu (27 and 8.4 nm min^{-1}, respectively). In order to obtain Cu-based alloys with a small content of Al, the exposed area of Al target was reduced by a shutter with a small aperture. Details of deposition parameters are listed in table 1. The film thickness was checked after deposition, using a DEKTAK stylus profiler. The substrate temperature was measured continuously during and after film deposition by means of a thermocouple spot-welded directly to a stripe similar to that used for stress measurement (for details see [10]).

Stress evolution during and after sputter deposition of the Cu–Al layers was investigated by means of *in situ* substrate curvature measurements using a laser-based optical bending beam technique. The details concerning construction and operation of the experimental set-up have been previously described [10, 11]. The substrate deflection is proportional to the force per unit width, F/w, which is equal to the product between the average stress $\langle\sigma\rangle$ and the film thickness t_f. It is calculated via Stoney's equation [12] from the change in the position of the two laser beams on the detectors Δ_1 and Δ_2 by

$$\frac{F}{w} = \langle\sigma\rangle t_f = -\frac{1}{12}\frac{E_s}{1-\nu_s}\frac{t_s^2}{d_b L}(\Delta_2 - \Delta_1)\,. \qquad (1)$$

$E_s/(1-\nu_s)$ and t_s are the biaxial modulus and thickness of the substrate, respectively, with $E_s/(1-\nu_s) = 180.5$ GPa and $t_s = 375$ μm. d_b and L denote the distance between the two parallel beams and the substrate–detector optical path, respectively ($d_b = 30$ mm, $L = 495$ mm).

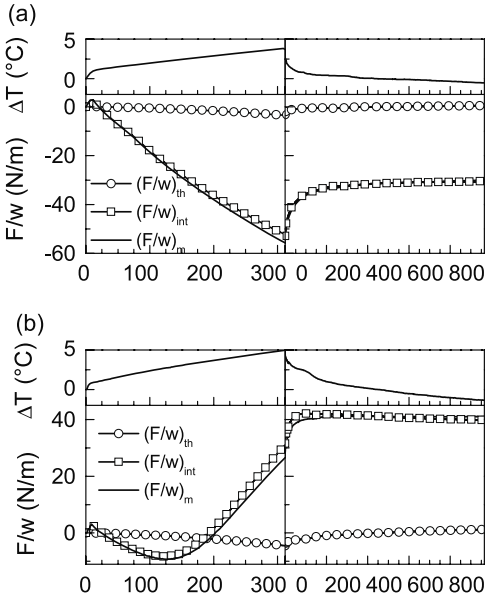

Figure 1. The change of the substrate temperature ΔT and the magnitude of the forces per unit width F/w—as measured $(F/w)_m$, thermal $(F/w)_{th}$, and intrinsic $(F/w)_{int}$—during and after sputtering of 300 nm thick Cu–Al alloy films at a sputter pressure of (a) 0.5 Pa, 1 at.% Al, and (b) 2 Pa, 2 at.% Al.

During co-sputtering of Cu and Al the substrate temperature increases by a few degrees with a slight dependence on the sputter pressure. Two examples of the substrate temperature change during and after sputtering of 300 nm thick Cu alloy films, (a) 1 at.% Al, 0.5 Pa and (b) 2 at.% Al 2 Pa, are shown in figure 1. The corresponding thermal stress of the Cu–Al films is calculated via the linear thermal expansion coefficients of Si and Cu at room temperature (RT; $\alpha_{Si} = 2.5 \times 10^{-6}$ K^{-1} and $\alpha_{Cu} = 17 \times 10^{-6}$ K^{-1}) and the biaxial modulus of Cu for the thin film ($E_f = 130$ GPa and $\nu_f = 0.34$ for polycrystalline Cu). For the calculations we used the value of the biaxial modulus for polycrystalline Cu because the electron backscattering diffraction (EBSD) revealed that our sputtered Cu films are truly polycrystalline with only a small (111) texture depending on the Ar pressure. Figure 1 also contains the corresponding thermal forces per unit width $(F/w)_{th}$ as well as the measured and thermally corrected intrinsic forces $(F/w)_m$ and $(F/w)_{int}$, respectively. Since the thermal corrections amount to only a few per cent of the intrinsic stress, in all other figures the raw data of the stress measurements are plotted.

The microstructure analyses of the sputtered films were performed *ex situ* with a focused ion beam system, 1540 XB, a FE-SEM Gemini 1530 (both Zeiss NTS) equipped with an EBSD-system CHANNEL 5 (HKL Technology), as well as a Veeco DI 3100 AFM. The SEM images were analyzed with our image analysis software NANOKORN2 for estimating island size (for details see [13]). The composition of the alloy-based layers was determined after deposition from the depth profile by glow discharge optical emission spectroscopy (GD-OES) and Auger electron spectroscopy (AES). It is in good

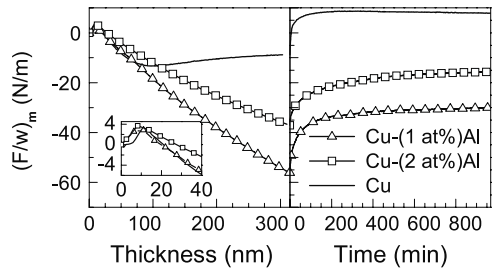

Figure 2. Evolution of the measured force per unit width $(F/w)_m$ during (left) and after (right) sputter deposition at 0.5 Pa of 300 nm thick Cu–Al alloy films (1 and 2 at.% Al) with the respective pure Cu film for comparison. The inset shows the evolution of $(F/w)_m$ during the early stages of deposition.

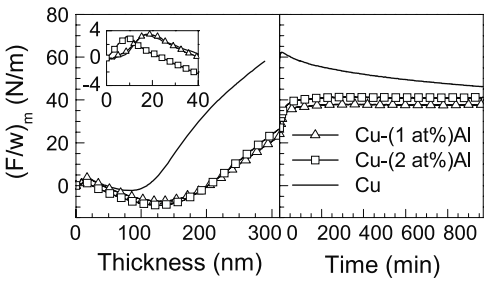

Figure 3. Evolution of the measured force per unit width $(F/w)_m$ during (left) and after (right) the sputter deposition at 2 Pa of 300 nm thick Cu–Al alloy films (1 and 2 at.% Al) with the respective pure Cu film for comparison. The inset shows the evolution of $(F/w)_m$ during the early stages of deposition.

agreement with the composition estimated from the ratio of the Cu and Al particle fluxes. Furthermore, AES depth profiles of Cu–(2 at.%)Al films deposited at sputter pressure of 0.5 and 2 Pa did not reveal incorporation of nitrogen, carbon and oxygen into the growing films; therefore the influence of these impurities on the mechanisms responsible for stress generation and relaxation is excluded. The electrical resistance of the samples was measured at RT by the van der Pauw method.

In order to explore the influence of the alloy composition and the sputter pressure on the film stress, the following different series of measurements were performed:

(1) Series I: Cu–Al films with a constant thickness of 300 nm and a fixed nominal Al content of 1 at.% have been deposited at sputter pressures of 0.5 and 2 Pa.
(2) Series II is analogous to series I; only the Al content is higher (2 at.%).
(3) Series III: thin Cu–Al films with thicknesses of 3, 5, 7, and 10 nm and a constant nominal Al content of 2 at.% have been deposited at a constant sputter pressure of 0.5 Pa.

3. Results

Figures 2 and 3 show the evolution of $(F/w)_m$ during and after sputter deposition of two Cu–Al alloy films with Al contents of 1 and 2 at.% together with that of a pure Cu film; the Ar pressure was 0.5 Pa and 2 Pa, respectively. The insets of figures 2 and 3 display higher resolution graphs of $(F/w)_m$ in the early stage of deposition. At the beginning of growth the film stress is tensile. $(F/w)_m$ increases with film thickness until a maximum is reached between 5 and 20 nm depending on the deposition parameters (see the insets). Compared to those for pure Cu films deposited at the same sputter pressure (0.5 and 2 Pa), the maximum is shifted to lower thicknesses indicating a reduced island size in the discontinuous alloy films. Upon further growth, a compressive stress dominates in the continuous films. For the alloy films sputtered at 2 Pa (figure 3), a further slope change in the $(F/w)_m$ curves from compressive to tensile stress is observed at a film thickness of ∼150 nm. For better clarity, the measured average stress $\langle\sigma\rangle_m$ of the Cu–Al alloy films calculated using equation (1) is displayed in figure 4. After finishing the deposition at

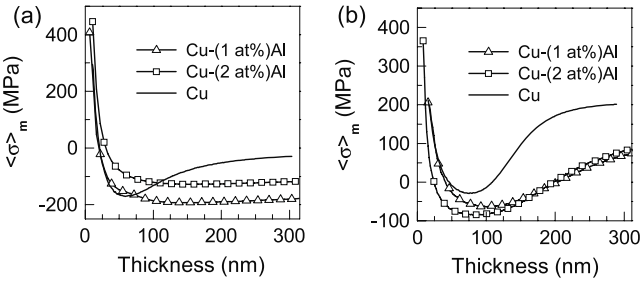

Figure 4. The evolution of the measured average stress $\langle\sigma\rangle_m$ during sputter deposition of Cu–Al alloy and Cu films at a constant Ar pressure of (a) 0.5 Pa and (b) 2 Pa, calculated using the experimental data of figures 2 and 3, respectively, for film thickness above 10 nm.

300 nm, the film stress continues to change for many hours (>16 h), leading to a tensile stress component in both the compressively stressed alloy films deposited at 0.5 Pa and the films under tensile stress prepared at the higher sputter pressure of 2 Pa. At 0.5 Pa the rate of the tensile stress generation decreases with increasing Al content. At 2 Pa, a short-term tensile stress change is followed by slow relaxation of tensile stress (figure 3). Comparing Cu–Al alloy films with the pure Cu film, the short-term development of the tensile stress is more pronounced and the long-term stress relaxation is almost negligible for alloy films.

The sequence of SEM images presented in figure 5(b) shows the surface morphology of thin Cu–Al (2 at.% Al) (left column) and Cu (right column) films at thicknesses of 3, 5, 7, and 10 nm. All films were deposited at an Ar pressure of 0.5 Pa. The morphology of the Cu–Al alloy layers is similar to that of the pure Cu film and reveals nucleation, island formation, percolation, and channel formation stages until the films become continuous. Figure 5(a) shows the stress curves of the two films measured with a higher sampling rate compared to figure 2. In agreement with the SEM results, the stress investigation indicates that the stage of the continuous alloy film is reached at a mean thickness of about 8 nm that is slightly lower than the corresponding thickness of the pure Cu film (∼10 nm).

Figure 6 shows FIB, SEM and AFM 3D images of the Cu–(1 at.%)Al films deposited at 0.5 and 2 Pa. The film thickness for both samples is 300 nm. Furthermore—

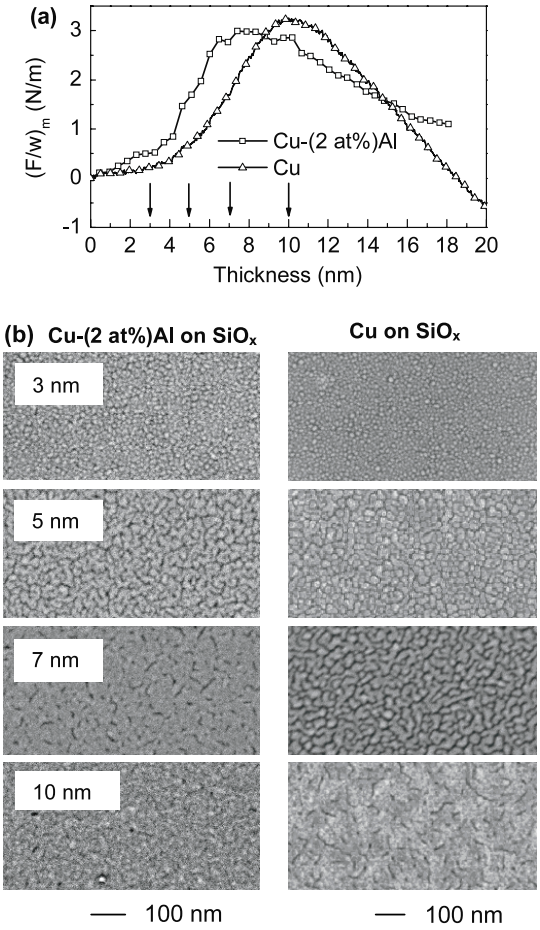

Figure 5. (a) Evolution of the measured force per unit width $(F/w)_{\mathrm{m}}$ during sputter deposition of a Cu–(2 at.%)Al and a Cu film at a sputter pressure of 0.5 Pa; arrows indicate the thickness at which the SEM images of (b) were taken. (b) Sequence of SEM images of the Cu–(2 at.%)Al (left column) and of respective Cu layers (right column) at thicknesses of 3, 5, 7, and 10 nm.

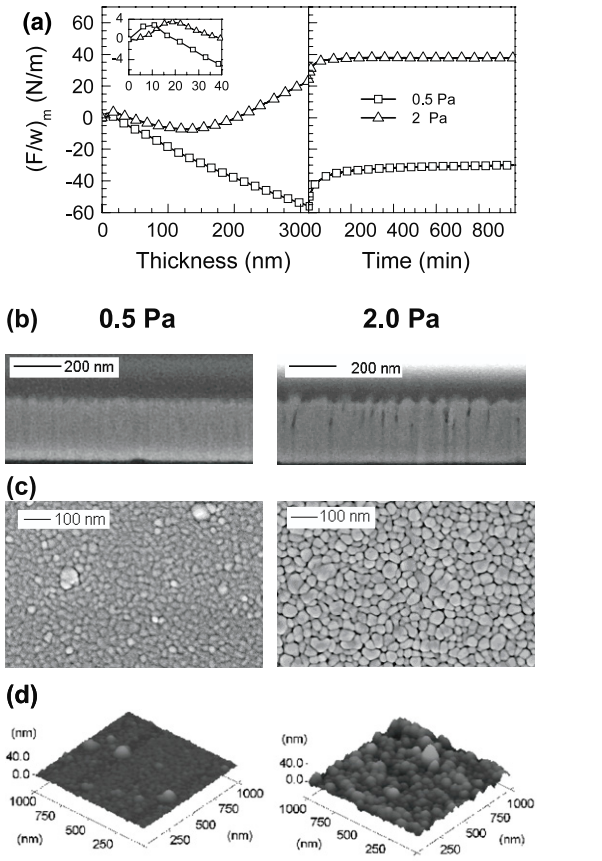

Figure 6. (a) Evolution of the measured force per unit width $(F/w)_{\mathrm{m}}$ during (left) and after (right) sputter deposition of 300 nm thick Cu–(1 at.%)Al films deposited at sputter pressures of 0.5 and 2 Pa; the inset shows the evolution of $(F/w)_{\mathrm{m}}$ during the early stages of deposition. (b) Cross-sectional FIB, (c) top-view SEM, and (d) AFM images of corresponding 300 nm thick Cu–(1 at.%)Al films deposited at Ar pressures of 0.5 (left column) and 2 Pa (right column).

for better comparison—the stress curves of the two films are plotted in figure 6(a). The cross-sectional FIB images (figure 6(b)) show a columnar grain structure for the two Cu–Al films. The grain size, like the surface roughness, is larger for the samples deposited at higher sputter pressure. Also, at the higher sputter pressure (2 Pa) and at thicknesses above 120 nm the grain boundaries appear more pronounced in the FIB images. The grain size estimated from SEM images for 15 nm thick films deposited at 0.5 Pa is about 25 nm. This value is increasing during deposition as is revealed in figure 6(c). Top-view images of both samples by SEM (figure 6(c)) reveal a uniform surface morphology with average lateral grain size of 43 and 63 nm. The morphological results are further corroborated by the AFM investigation (figure 6(d)). Evaluation of the height profiles confirms the increase of surface roughness with increasing sputter pressure (from 2 to 5 nm) indicated by cross-sectional FIB images.

The results of the microstructure investigations and resistivity data of Cu–Al alloys and pure Cu films are summarized in table 2. It is noteworthy that we could not deduce the grain size from EBSD measurements because no diffraction patterns were obtained, which may hint towards very small and/or distorted crystallites.

Table 2. Microstructure and resistivity data of the 300 nm thick Cu–Al alloy and Cu films deposited at sputter pressures of 0.5 and 2 Pa; grain size has been derived from SEM images; the surface roughness is given by root mean square (RMS) value determined for 1×1 μm^2 areas of the AFM images.

		Sputter pressure (Pa)	
	Materials	0.5	2
Grain size (nm)	Cu–(1 at.%)Al	43	63
	Cu–(2 at.%)Al	49	62
Surface roughness (RMS) (nm)	Cu–(1 at.%)Al	2.0	5.0
	Cu–(2 at.%)Al	3.0	4.5
	Cu	1.5	3.0
Resistivity (10^{-8} Ω m) at RT	Cu–(1 at.%)Al	3.9	4.9
	Cu–(2 at.%)Al	4.6	5.2
	Cu	2.1	2.5

4. Discussion

The growth of Cu–Al films on SiO_x substrates proceeds in the Volmer–Weber (VW) mode, like for pure Cu films. This is suggested by the thickness dependence of the stress displayed in figures 2 and 3 with tensile maxima in the force curves at film thicknesses between 7 and 20 nm. The nucleation of discrete islands, island growth, and coalescence in accordance with the VW growth is confirmed by the sequence of SEM images presented in figure 5. Therefore the growth of the magnetron sputtered Cu–Al alloy films is consistent with the growth of the recently investigated sputtered Cu [10] and Co [11] single layers and Co/Cu [13] multilayers, which all grow in the VW mode. More generally, the film stress corresponds to that of polycrystalline metal films with high mobility. In the coalescence stage a large tensile stress develops due to the formation of grain boundaries [14–17], which levels off when the films become continuous, as well as recrystallization of already merged grains [18]. As discussed in [19], the tensile maximum in F/w curves indicates the thickness at which VW films become continuous and therefore is directly related to island density in the discontinuous film and average island size at percolation. At a sputter pressure of 0.5 Pa there is only a weak dependence of the position of the maximum on the Al content with a slight shift to lower thickness for the 2 at.% Al film. The maximum of the 2 at.% Al alloy film is also shifted to lower thickness compared to that for the pure Cu film indicating a reduction of the surface mobility with increasing Al content. An analogous trend is observed at the higher sputter pressure of 2 Pa. Interestingly, however, the increase of the sputter pressure leads to an overall shift of the $(F/w)_m$ maxima to larger thicknesses, consistently with the increase in grain size observed by SEM and FIB.

In the continuous films a compressive stress contribution is dominating, which is responsible for the reversal of the slope of the $(F/w)_m$ curves after the tensile maximum. When growth proceeds the compressive stress contribution weakens until the tensile stress in the films prevails—as in the case of the pure Cu and for the Cu–(2 at.%)Al films deposited at a sputter pressure of 2 Pa. According to [18], grain growth during film growth is responsible for the relaxation of the compressive stress and generation of tensile stress during deposition.

We discuss now the mechanisms responsible for the generation of the compressive stress after percolation. Three models have been proposed in the literature for explaining the occurrence of compressive stress in continuous films. (i) For evaporated VW films it has been proposed that a compressive strain field, generated in the island stage by capillarity effects [20–23], is propagated into the continuous film upon further growth [24]. The strain field increases with decreasing island size at percolation and decreases with film thickness due to incorporation of defects (voids, dislocations, grain boundaries, vacancies, point defects). The latter effect leads to a reversal of the stress from compressive to tensile in thicker films, particularly upon high vacuum deposition [24]. (ii) Chason *et al* [25] suggested a flux-driven incorporation of excess atoms in grain boundaries during deposition due to the chemical potential of the growth surface being higher than that of grain boundaries. (iii) For sputtered VW films, 'the atomic peening' effect of the energetic particles striking the film produces the lattice distortions during film growth [26, 27]. Due to reduced thermalization, the development of the compressive stress is more intense at lower Ar pressure (here at 0.5 Pa). Model (i) is fully consistent with the experimental results, but on the basis of our experiments we cannot exclude the contributions of the incorporation of the excess atoms in grain boundaries and 'the atomic peening' effects accounted for in models (ii) and (iii), respectively.

According to our SEM and FIB investigations, the grains continue to grow laterally in the continuous films leading to a V-shaped columnar morphology of sputtered films as is typical for high mobility metals. It is known that additives can promote or inhibit the phenomena of structure formation (i.e., nucleation, crystal growth, grain growth) [28]. For instance, the refinement in grain size upon introduction of an alloying element (or impurity) can be ascribed to the reduction of the surface and bulk atom mobilities as well as repeated grain nucleation during deposition [29, 30]. In the case of the Cu–Al alloy films, the addition of Al leads to a considerable reduction of the grain size. Compared to the case for 300 nm thick pure Cu films with average grain sizes of 360 and 290 nm (determined from FIB top views in [10]) at sputter pressures of 0.5 and 2 Pa, respectively, the grain size is reduced by a factor of 5–6 (see table 2). Obviously, Al inhibits grain growth responsible for the relaxation process during and after film growth [18], thus acting as a 'refiner' for Cu. After finishing deposition, short-term (∼min) stress changes may have their origin in a reversible change of the grown surface [25, 31, 32]. For the long-term stress changes the following mechanisms may be responsible: (i) plastic deformation, e.g., dislocation-mediated plasticity [33] that is controlled by dislocation glide at low homologous temperature T_s/T_m (ratio of substrate versus melting temperature) and high level of stress as well as the diffusion-mediated plasticity [34] that is controlled by diffusion along surface and grain boundaries (Coble creep) at low T_s/T_m and low level of stress; (ii) change of the microstructure due to recrystallization [32, 35]. Because of the high level of stress and low T_s/T_m, we speculate that the dislocation glide plays the main role in the stress relaxation behavior for the films deposited at 0.5 and 2 Pa. Further investigations of the microstructure development in defined time intervals after deposition are necessary to unambiguously clarify the mechanisms of post-growth stress development.

It is noteworthy that the results on microstructure development and surface topography of the Cu–Al films as a function of sputter pressure are in agreement with the structure zone model (SZM) developed by Thornton [36] and extended by Mahieu *et al* [37]. According to the SZM developed by Thornton, for the homologous temperature of Cu, $T_s/T_m = 300/1356 = 0.22$, two different structural morphologies are dominant at high and low sputtering pressures, respectively: Zone-1 is characterized by columnar crystallites defined by open boundaries, and Zone-T by a dense array of poorly defined fibrous grains. A transition from Zone-1 to Zone-T occurs as the sputtering pressure decreases. According to the Thornton model, microstructure evolution can be correlated

with stress development. For the region of the compressive stress (0.5 Pa), the films should exhibit a relatively dense microstructure and smooth surfaces. For the region of the tensile stress (2 Pa), the films are characterized by an open microstructure and higher surface roughness, in agreement with our findings.

Furthermore, the evolution from a relatively dense to a more open microstructure is correlated with the increase of the electrical resistivity. At RT the resistivity of the Cu–(1 at.%)Al and Cu–(2 at.%)Al films increases from 3.9×10^{-8} to 4.9×10^{-8} Ω m and from 4.6×10^{-8} to 5.2×10^{-8} Ω m, respectively, upon increasing of sputter pressure from 0.5 to 2 Pa.

5. Conclusions

We investigated the stress and microstructure of up to 300 nm thick dilute Cu–Al alloy films containing 1 and 2 at.% Al by means of substrate curvature measurements, FIB, SEM, and AFM. The films were DC magnetron sputtered onto SiO_x substrates at Ar pressures 0.5 and 2 Pa. At both sputter pressures and for both Al concentrations, film growth proceeds in the VW mode with a stress evolution typical for high mobility metals. Increase of the Al content from 1 to 2 at.% leads to finer-grained films indicating that Al reduces the overall adatom mobility of the film. Moreover, the average grain size depends on the sputter pressure and increases, e.g., for 300 nm thick Cu–(1 at.%)Al films from 43 to 63 nm at 0.5 and 2 Pa, respectively. Upon raising the sputter pressure from 0.5 to 2 Pa, the stress in thicker films (>150 nm) switches from compressive to tensile; this is accompanied by a change from a relatively dense to an open microstructure. In all cases the average grain size increases with film thickness during growth. Even after finishing deposition, in all films a tensile stress contribution is observed that continues to increase for many hours, thus pointing to ongoing restructuring of the films. Our results therefore suggest that higher Al contents may be necessary for suppressing grain growth in Cu–Al alloys.

Acknowledgments

The authors would like to thank W Brückner for a critical reading of the manuscript and for useful suggestions, S Baunack for AES investigations, V Hoffmann for GD-OES analysis, B Eichler for AFM investigations, A Weckbrodt for resistivity measurements, and I Fiering and C Krien for technical assistance.

References

[1] Park C W and Vook R W 1991 *Appl. Phys. Lett.* **59** 175
[2] Diamand Y S, Dubin V and Angyal M 1995 *Thin Solid Films* **262** 93
[3] Muraka S P 1997 *Mater. Sci. Eng.* R **19** 87
[4] The International Technology Roadmap for Semiconductors (ITRS) 2002 update www.itrs.net/Links/2002Update/
[5] Barmak K, Cabral C, Rodbell K P and Harper J M E 2006 *J. Vac. Sci. Technol.* B **24** 2485
[6] Ding P J, Lanford W A, Hymes S and Murarka S P 1994 *J. Appl. Phys.* **75** 3627
[7] Musil J, Bell A J, Cepera M and Zeman J 1997 *J. Surf. Coat. Technol.* **96** 359
[8] Wang P I, Muraka S P, Kaminski D A, Bedell S and Lanford W A 2001 *J. Electrochem. Soc.* **148** G481
[9] Barmak K, Gungor A, Rollet A D, Cabral C and Harper J M E 2003 *Mater. Sci. Semicond. Process.* **6** 175
[10] Pletea M, Brückner W, Wendrock H and Kaltofen R 2005 *J. Appl. Phys.* **97** 054908
[11] Pletea M, Brückner W, Wendrock H, Kaltofen R and Koch R 2006 *J. Appl. Phys.* **99** 033509
[12] Stoney G G 1909 *Proc. R. Soc.* A **82** 172
[13] Pletea M, Brückner W, Wendrock H, Thomas J, Kaltofen R and Koch R 2007 *J. Appl. Phys.* **101** 073511
[14] Doljack F A and Hoffman R W 1972 *Thin Solid Films* **12** 71
[15] Nix W D and Clemens B M 1999 *J. Mater. Res.* **14** 3467
[16] Seel S C, Thompson C V, Hearne S J and Floro J A 2000 *J. Appl. Phys.* **88** 7079
[17] Freund L B and Chason E 2001 *J. Appl. Phys.* **89** 4866
[18] Chaudhari P 1971 *J. Vac. Sci. Technol.* **9** 520
[19] Koch R 1994 *J. Phys.: Condens. Matter* **6** 9519
[20] Finegan J D and Hoffman R W 1961 *AEC Technical Report* 18 (Cleveland, OH: Case Institute of Technology)
[21] Abermann R, Kramer R and Mäser J 1978 *Thin Solid Films* **52** 215
[22] Cammarata R C, Trimble T M and Srolovitz D J 2000 *J. Mater. Res.* **15** 2468
[23] Floro J A, Hearne S J, Hunter J A, Kotula P, Chason E, Seel S C and Thomson C V 2001 *J. Appl. Phys.* **89** 4886
[24] Abermann R, Koch R and Kramer R 1979 *Thin Solid Films* **58** 365
[25] Chason E, Sheldon B W, Freund L B, Floro J A and Hearne S J 2002 *Phys. Rev. Lett.* **88** 156103–1
[26] D'Heurle F M 1970 *Metall. Trans.* **1** 725
[27] Windischmann H J 1991 *J. Vac. Sci. Technol.* A **9** 2431
[28] Barna P B and Adamik M 1998 *Thin Solid Films* **317** 27
[29] Frear D R, Sanchez J E, Romig A D and Morris J W 1990 *Metall. Trans.* A **21** 2449
[30] Petrov I, Barna P B, Hultman L and Greene J E 2003 *J. Vac. Sci. Technol.* A **21** S117
[31] Spaepen F 2000 *Acta Mater.* **48** 31
[32] Koch R, Hu D and Das A K 2005 *Phys. Rev. Lett.* **94** 146101
[33] Kraft O, Freund L B, Philips R and Arzt E 2002 *MRS Bull.* **27** (January) 30
[34] Josell D, Weihs T P and Gao H 2002 *MRS Bull.* **27** (January) 39
[35] Koch R and Abermann R 1986 *Thin Solid Films* **140** 217
[36] Thornton J A 1977 *Annu. Rev. Mater. Sci.* **7** 239
[37] Mahieu S, Ghekiere P, Depla D and De Gryse R 2006 *Thin Solid Films* **515** 1229